2D Materials

PAPER

Gas dependent hysteresis in MoS_2 field effect transistors

To cite this article: Francesca Urban *et al* 2019 *2D Mater.* **6** 045049

2D Materials

RECEIVED
14 June 2019

REVISED
22 August 2019

ACCEPTED FOR PUBLICATION
30 August 2019

PUBLISHED
23 September 2019

PAPER

Gas dependent hysteresis in MoS_2 field effect transistors

Francesca Urban[1,2], Filippo Giubileo[2], Alessandro Grillo[1], Laura Iemmo[1,2], Giuseppe Luongo[1,2], Maurizio Passacantando[3], Tobias Foller[4], Lukas Madauß[4], Erik Pollmann[4], Martin Paul Geller[4], Dennis Oing[4], Marika Schleberger[4] and Antonio Di Bartolomeo[1,2,5]

[1] Physics Department 'E. R. Caianiello', University of Salerno, via Giovanni Paolo II n. 132, Fisciano 84084, Italy
[2] CNR-SPIN Salerno, via Giovanni Paolo II n. 132, Fisciano 84084, Italy
[3] Department of Physical and Chemical Science, University of L'Aquila, CNR-SPIN L'Aquila, via Vetoio, Coppito 67100, L'Aquila, Italy
[4] Faculty of Physics and CENIDE, University of Duisburg-Essen, Lotharstraße 1, Duisburg 47057, Germany
[5] Interdepartmental Centre NanoMates, University of Salerno, via Giovanni Paolo II n. 132, Fisciano 84084, Italy

E-mail: adibartolomeo@unisa.it **and** marika.schleberger@uni-due.de

Keywords: MoS_2, field effect transistor, hysteresis, gas adsorption, memory

Abstract

We study the effect of electric stress, gas pressure and gas type on the hysteresis in the transfer characteristics of monolayer molybdenum disulfide (MoS_2) field effect transistors. The presence of defects and point vacancies in the MoS_2 crystal structure facilitates the adsorption of oxygen, nitrogen, hydrogen or methane, which strongly affect the transistor electrical characteristics. Although the gas adsorption does not modify the conduction type, we demonstrate a correlation between hysteresis width and adsorption energy onto the MoS_2 surface. We show that hysteresis is controllable by pressure and/or gas type. Hysteresis features two well-separated current levels, especially when gases are stably adsorbed on the channel, which can be exploited in memory devices.

Introduction

During the last few years, there has been an increasing interest in two-dimensional (2D) materials for technological applications. The presence of a tunable and layer-sizable bandgap, the mechanical strength and the chemical and thermal stability make 2D transition metal dichalcogenides (TMDs) good candidates for next-generation electronic devices [1–6]. Theoretical and experimental studies have demonstrated that 2D TMDs based devices can achieve carrier mobilities up to hundreds $cm^2\,V^{-1}\,s^{-1}$, very high on/off ratios up to 10^8, low power consumption and short switching times [7–14]. In their 2D form, owing to the low density of states, TMDs enable enhanced gate control in easy-to-fabricate transistors immune from short-channel effects. Indeed, compared to silicon traditional devices, TMD field-effect transistors (FET) show steeper subthreshold swing (SS), negligible drain-induced barrier lowering (DIBL), high drive current capabilities and low standby off-current, even when relatively thick gate oxides are used [15, 16]. The control of *n*- or *p*-type conduction is another important advantage offered by TMDs transistors. Indeed, ambipolar conduction and high on/off ratio are important features for stable low-power consumption and performant logic applications [17, 18]. Furthermore, TMDs can be integrated into silicon fabrication technologies to realize devices with nanometric channel length, suitable for high-density integrated circuits.

Additional features like photoconduction [6, 19] and spin-orbit splitting [20] have been investigated for optoelectronic and spintronic applications [21]. Moreover, the sharp edges of TMD flakes, combined with intrinsic doping and low electron affinities, make TMDs promising materials also for field emission devices for vacuum electronics applications [22–29].

Owing to the high surface-to-volume ratio, TMDs have excellent sensing performances. The MoS_2 sensitivity to NO and NO_2 has been demonstrated [30] with a detection limit of 0.8 ppm, but the exposure to other gases (studied from the theoretical point of view [31, 32]) remains experimentally unexplored.

A considerable number of studies have been also devoted to the effects of the environment on mono- and few-layer TMD devices [33, 34]. For instance, it has been shown that WSe_2 is very sensitive to pressure which can tune the conduction type [33]. Similarly, $PdSe_2$, which is a relatively new 2D material, has been demonstrated to be a good gas and pressure sensor [34].

A major difficulty that TMD-based nanoelectronics has to overcome is related to point defects as well as structural damages and dislocations, often generated during the fabrication, independently of the used process such as chemical vapor deposition (CVD) or mechanical exfoliation. Structural defects behave as charge traps and scattering centers, which modify the electronic properties of the devices and generate unwanted hysteresis and/or reduction of conductivity [3, 35, 36]. Hysteresis consists of a shift of the transistor transfer characteristic for consecutive forward/reverse gate voltage sweeps and changes the threshold voltage; it is an unwanted effect to circuits' designers, as it makes the transistor dependent on the biasing history. In spite of that, hysteresis can be conveniently exploited for the fabrication of memory devices [37–39], since it features two distinct and stable states, that can be used to define the bits of a memory cell. In this regard, it is interesting and important to understand the physical properties that control the hysteretic behavior of the transfer characteristic in TMD transistors.

In this paper, the electric properties of CVD-grown monolayer MoS_2 field effect transistors are studied under external stimuli, such as gate voltage, sweep delay time, pressure and pure gas environment, with particular attention to hysteresis. MoS_2 was selected among other TMDs because of his layer dependent bandgap over a wide range (1.2–1.9 eV), stability in air and mobility of few tens $cm^2\ V^{-1}\ s^{-1}$ when deposited on SiO_2 [4, 7, 8, 40].

Chalcogen vacancies favor a natural n-type doping in MoS_2 and act as trap centers that enhance the hysteretic behavior in MoS_2 and others 2D TMDs [19, 34, 41]. We demonstrate exponential dependence of the hysteresis on the sweeping time and a linear dependence on the gate voltage range. We also show that exposure to gases such as oxygen, nitrogen and hydrogen at different pressure modifies the electrical properties of the devices [42], a feature that can be exploited for gas sensing purposes. In addition we prove that defective MoS_2 flakes are strongly sensitive to gases like methane (CH_4), as anticipated by DFT (density functional theory) studies [43]. We finally show that the wide hysteresis, especially if enhanced by gas adsorption, enables a two-bit memory device featuring a charge retention on the time scale of several minutes and an endurance on the order of hundreds of cycles.

Methods

The MoS_2 flakes were grown in a three-zone split tube furnace (ThermConcept), purged with 500 N $cm^3\ min^{-1}$ of Ar gas for 15 min to minimize the O_2 content. The growing Si/SiO_2 substrate was spin coated with a 1% sodium cholate solution, then a saturated ammonium heptamolybdate (AHM) solution served as the molybdenum feedstock. The target material was placed in one zone of the three-zone tube furnace along with 50 mg of S powder, positioned upstream in a separate heating zone. The zone containing the S and AHM were heated to 150 °C and 750 °C, respectively. After 15 min of growth, the process was stopped, and the sample was cooled rapidly.

Raman and atomic force microscopy (AFM) measurements were used to identify monolayer MoS_2 among the randomly distributed CVD-grown flakes. Using the substrate as common back-gate, we realized back-gated transistors by evaporating the drain and source electrodes on selected single layer flakes (see figure 1) by means of standard photolithography and lift-off process.

The contacts were made of Ti (10 nm) and Au (100 nm), deposited as adhesion and cover layers, respectively.

In the following, the electrical characterization refers to the inner contacts 1 and 2 as displayed in figure 1(a). Measurements were carried out inside a scanning electron microscope chamber (SEM, LEO 1530, Zeiss), equipped with two metallic tips, with curvature radius of about 100 nm (figure 1(b)) and nanometric positioning capability, connected to a Keithley 4200 SCS (source measurement units, Tektronix Inc.), at room temperature and different chamber pressures, from $\sim 10^{-6}$ Torr to 760 Torr.

The selected flake was characterized by AFM and Raman/photoluminescence (PL) measurements (Renishaw InVia Raman spectrometer with 532 nm laser wavelength). The results shown in figures 1(c) and (d) prove that the flake is a single layer, as both the step height of ~ 0.75 nm and the large PL peak at ~ 1.85 eV, correspond to the typical height and bandgap values for a monolayer. We note that PL intensity and the AFM step height point to absence of intercalated water at the SiO_2/MoS_2 interface, owing to high growth temperatures of 750 °C.

Results

The electrical characterization of the device starts with the output and transfer characteristics, as shown in figure 2, measured at 10^{-6} Torr. To avoid device damage, the channel current and the gate voltage were limited to 1 μA and 50 V, respectively. The output characteristics of figure 2(a) show a slightly rectifying behavior typical of TMD transistors, where Schottky barriers between the channel and the contacts are easily formed [35–37]. Figure 2(b) confirms a normally-on n-type transistor with on/off ratio of ~6 orders of magnitude, featuring a subthreshold swing $SS = \frac{d(V_{gs})}{dLog(I_{ds})} \sim 1\ V/dec$.

From the relation between mobility and gate voltage, $\mu = \frac{dI_{ds}}{dV_{gs}} \frac{L}{W C_{ox} V_{ds}}$, where C_{ox} is the SiO_2 capacitance per unit area (11 nF cm^{-2} for an oxide thickness of 300 nm), V_{ds} the voltage bias and dI_{ds}/dV_{gs} the transconductance (obtained as the slope of the transfer characteristic at high V_{gs}), we derived a mobility of $\sim 1\ cm^2\ V^{-1}\ s^{-1}$.

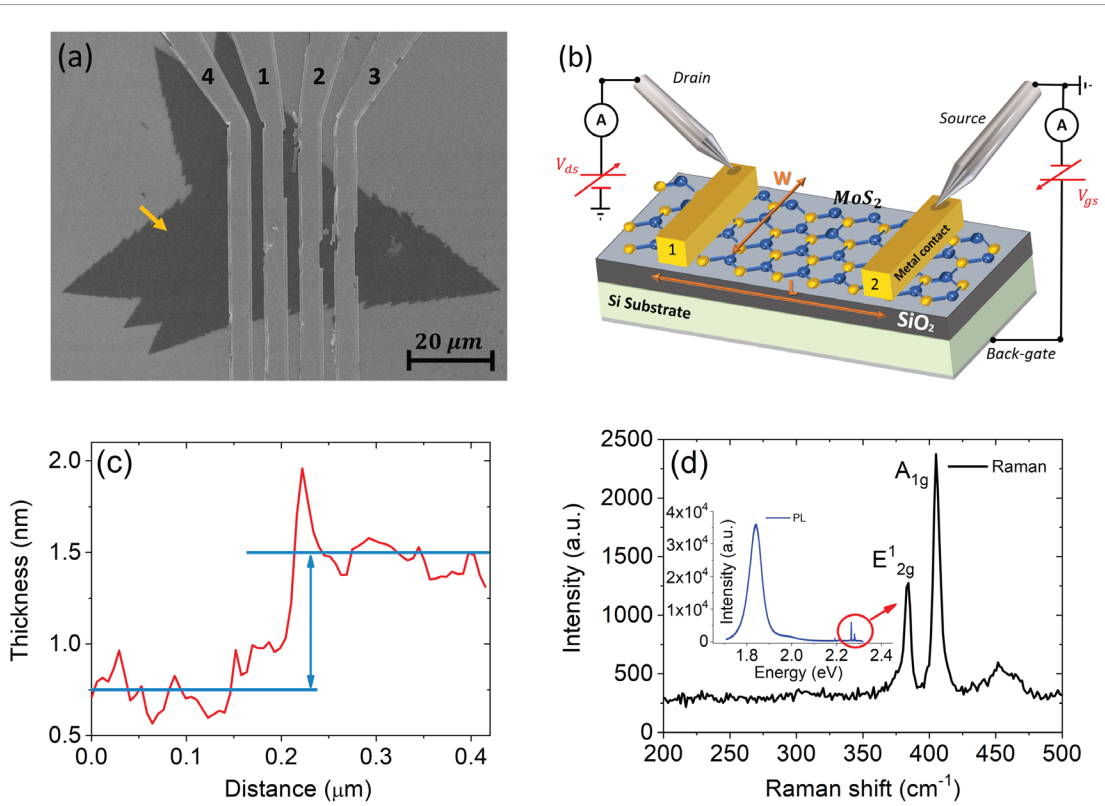

Figure 1. (a) SEM image of the selected flake with Ti/Au contacts; the yellow arrow indicates the AFM measurement direction. (b) Schematic of the device and the measurement setup; contacts 1 and 2 were chosen as the drain and source electrodes while scratched silicon substrate, covered with silver paint, operated as the back gate. The white arrows indicate the channel length ($L \sim 5$ μm) and width ($W \sim 40$ μm) of the device. (c) AFM measurement of the step height between the substrate and the flake. (d) Raman spectrum showing E^1_{2g} and A_{1g} modes separated by ~ 20 cm^{-1}, typical of a monolayer MoS_2; the inset displays a photoluminescence peak at ~ 1.85 eV energy bandgap, as expected for a monolayer.

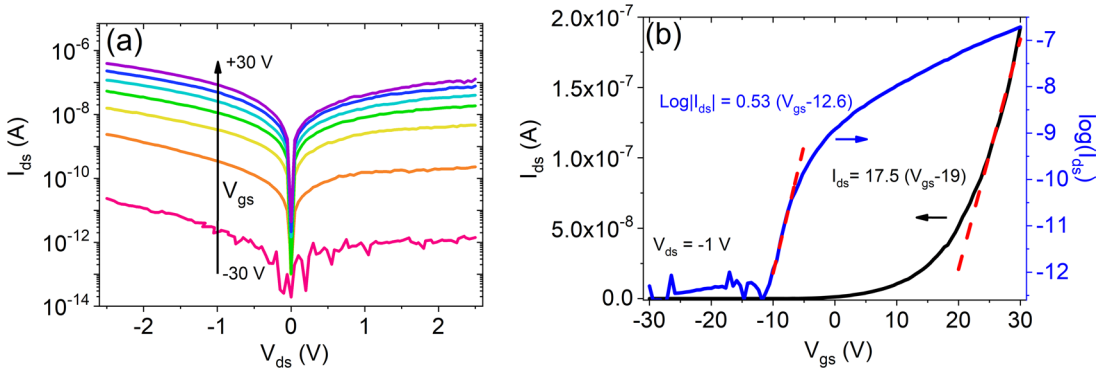

Figure 2. (a) Output and (b) transfer characteristics, measured at 10^{-6} Torr between contacts 1 and 2.

This slightly low mobility, likely worsened also by the contact resistance [44–46], suggests the presence of trap states. Three types of trap states can be distinguished, as illustrated in figure 3(a): The adsorbates on the MoS_2 surface (1), the intrinsic defects in the crystal structure of MoS_2 (2), and the extrinsic traps at the MoS_2/SiO_2 interface or into the SiO_2 dielectric layer (3). Each trap state is characterized by a trapping/detrapping time constant, which can be evaluated by several techniques.

A long annealing in high vacuum can remove most of the adsorbates (1) and allow the investigation of the effect of traps (2) and (3) only.

The transfer curve measured after 24 h at 25°C and $\sim 10^{-6}$ Torr shows a clockwise hysteretic behavior when the gate voltage is swept forth and back (figure 3(b)). The right-shift of the transfer after a forward V_{gs} sweep corresponds to negative charge trapping. Hysteresis can be characterized by a hysteresis width, H_W, defined as the difference of the gate voltages corresponding to the current of 0.1 nA. The hysteretic behavior is investigated as a function of the gate voltage range and the sweeping time in figures 3(c) and (d). A linear dependence of H_W on the gate voltage range is shown in the inset of figure 3(c), while an exponential growth of H_W with the sweeping time is reported in figure 3(e). The

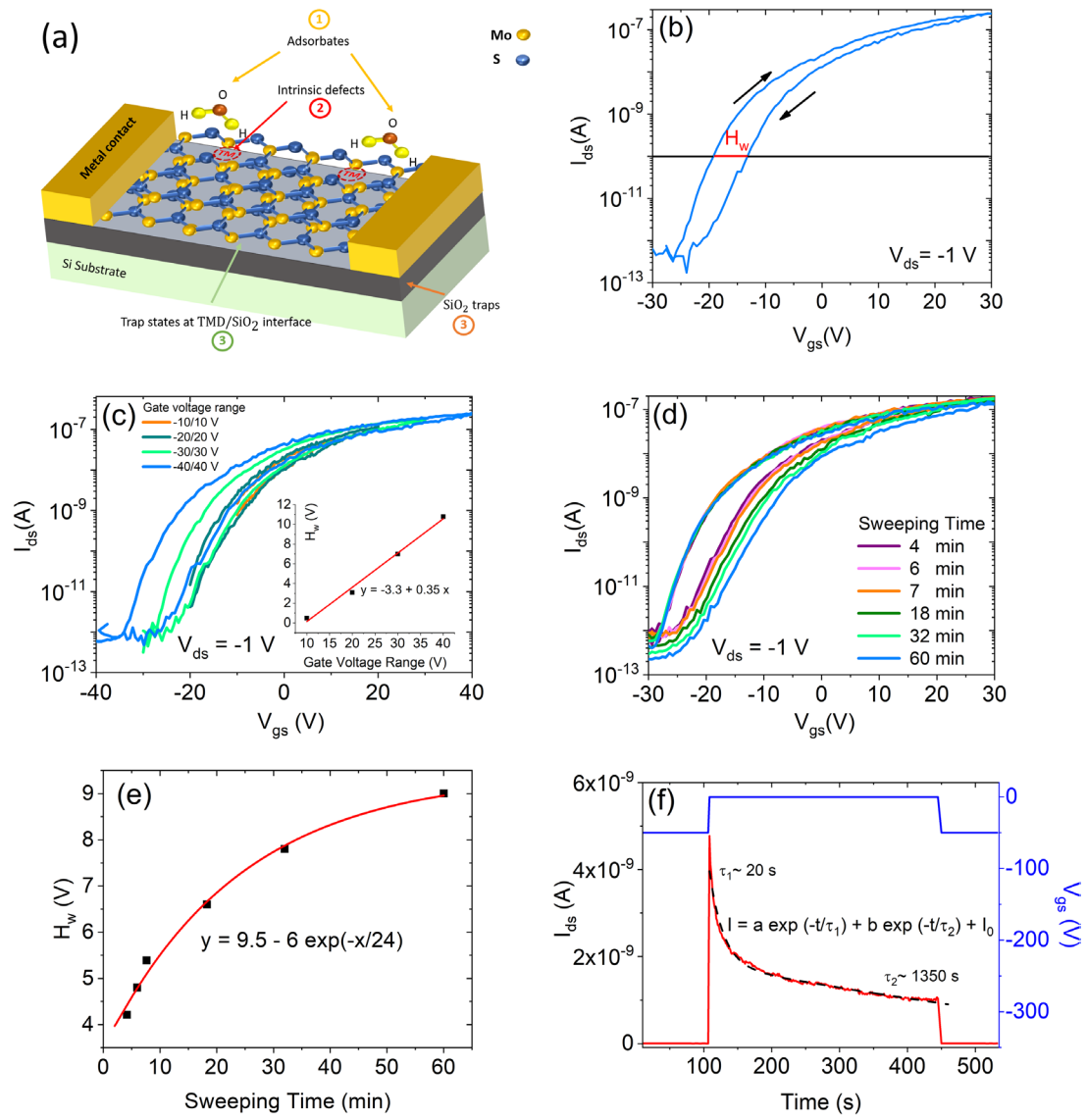

Figure 3. (a) Schematic of the different types of trap states present in a back-gate, unprotected MoS_2 transistor. (b) Transfer characteristic after 24 h anneal at 25 °C temperature and ~10^{-6} Torr pressure. (c) Dependence of the transfer characteristic on the gate voltage range (the inset show the linear dependence of H_W), and (d) on sweeping time. (e) Exponential behavior of the hysteresis width as function of the sweeping time. (f) Experimental data (red curve) and fitting curve (black dashed) for the transient behavior of the transistor current during a gate pulse (blue curve) from −50 V to 0 V (at $V_{ds} = -1$ V).

linear increase of H_W with the gate voltage range indicates that the trapped charge is proportional to gate potential, as expected considering that the trapping process load the capacitor formed by the MoS_2 channel and the Si substrate. The exponential growth of H_W with the sweeping time [47] characterized by a long time constant of ∼ 24 min, indicates a predominant role of slow (deep) traps either in MoS_2 or in the SiO_2 insulator (see (2) and (3) in figure 3(a)).

More insight can be gained observing the transient behavior of the device under a gate voltage pulse. Figure 3(f) shows the channel current during a gate pulse of height 50 V and width ~400 s. The best fit is provided by a double exponential decay, $I_{ds} = a \exp\left(-\frac{t}{\tau_1}\right) + b \exp(-\frac{t}{\tau_2})$, characterized by decay constants $\tau_1 \sim 20$ s and $\tau_2 \sim 1350$ s (i.e. ~23 min), respectively. Such a behavior points to the presence of two types of electron trap states. The faster trapping is related to MoS_2 defects or MoS_2/SiO_2 interface trap states [48–50], while the slower trapping is ascribed to the filling of trap states inside the SiO_2 dielectric, controlled by the gate circuit. The exponential behavior of H_W with the sweeping time indicates that the slower component is dominant when slow gate sweeps are applied. Following the procedure proposed by Xu *et al* [35], we estimated a density of trap state in the MoS_2 structure of ∼ 10^{12} cm^{-2} eV^{-1} in agreement with other values reported in literature [51], using the transfer of figure 3(b), corresponding to the fastest sweep (4 min).

We consider now the role of adsorbates by injecting several types of pure gases in the SEM chamber and investigating their effect on the electrical properties of the device.

We start monitoring the variation of transfer characteristic at different O_2 pressures (figure 4(a)), as

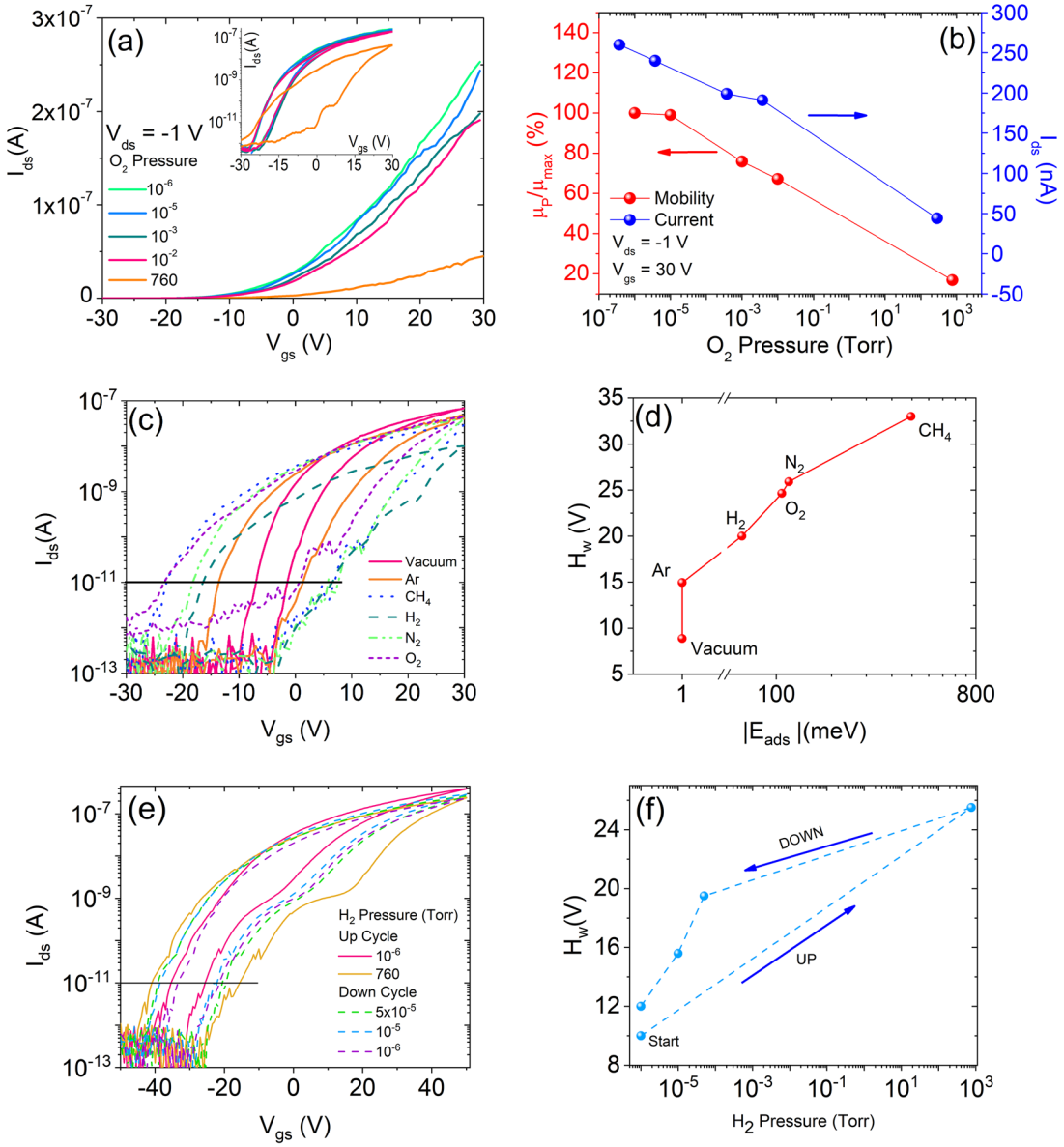

Figure 4. (a) Transfer characteristics at different O_2 pressures. (b) On-current (at $V_{gs} = 30$ V and $V_{ds} = -1$ V) and field effect mobility versus gas pressure. (c) Transfer characteristics measured under different gas atmospheres (Ar, H_2, O_2, N_2 and CH_4) at 760 Torr and in vacuum ($<10^{-6}$ Torr). (d) Hysteresis width versus gas adsorption energy on MoS_2 (E_{ads} for H_2 and O_2 from [31], N_2 from [54], CH_4 from [43]), as obtained from the sets of $I_{ds} - V_{gs}$ curves corresponding to $-30\ \text{V} \leqslant V_{gs} \leqslant 30$ V (figure (c)). Given the linear relation between hysteresis width and gate voltage range (displayed in figure 3(c)), we note that the $H_W - |E_{ads}|$ trend does not change for different gate voltage range choices. For display purposes, the adsorption energy corresponding to Ar and vacuum are set to 1 meV (no estimation of the E_{ads} is currently available for Ar–MoS_2 system, while it results in the range 1–10 meV for Ar-carbon allotrope systems [56]). (e) Transfer characteristics and (f) hysteresis width when the pressure is raised from 10^{-6} Torr to 760 Torr and then decreased to 10^{-6} Torr, in H_2 environment.

metrics to check its effect we chose the on-current and the channel mobility, as shown in figure 4(b).

A monotonic change of the conduction parameters occurs while raising the pressure from 10^{-6} to 760 Torr. When the chamber is brought to atmospheric pressure in O_2 environment, a reduction of the on-current of one order of magnitude and an 80% decrease of the mobility are observed, owing to the adsorption of oxygen. Being highly electronegative, oxygen has an acceptor nature and traps electrons. This reduces the FET current and increases the coulomb scattering that degrades the channel mobility [36]. The compressive stress, applied by pressure to the MoS_2 channel, favors the interaction with the supporting SiO_2 dielectric and acts as a further mobility suppressor. The increased interaction with the substrate also facilitates charge transfer and contributes to hysteresis (see inset of figure 4(a)).

Figure 4(c) shows the transfer characteristics measured in vacuum (~10^{-6} Torr, solid pink curve) and in 760 Torr atmospheres of pure Ar, H_2, O_2, N_2 and CH_4, respectively. Such gases where chosen because of their great interest for gas detection and storage applications and for the availability of theoretical results based on DFT calculations.

The hysteresis can be related to the adsorption energy (E_{ads}) of the various gases, defined as the difference

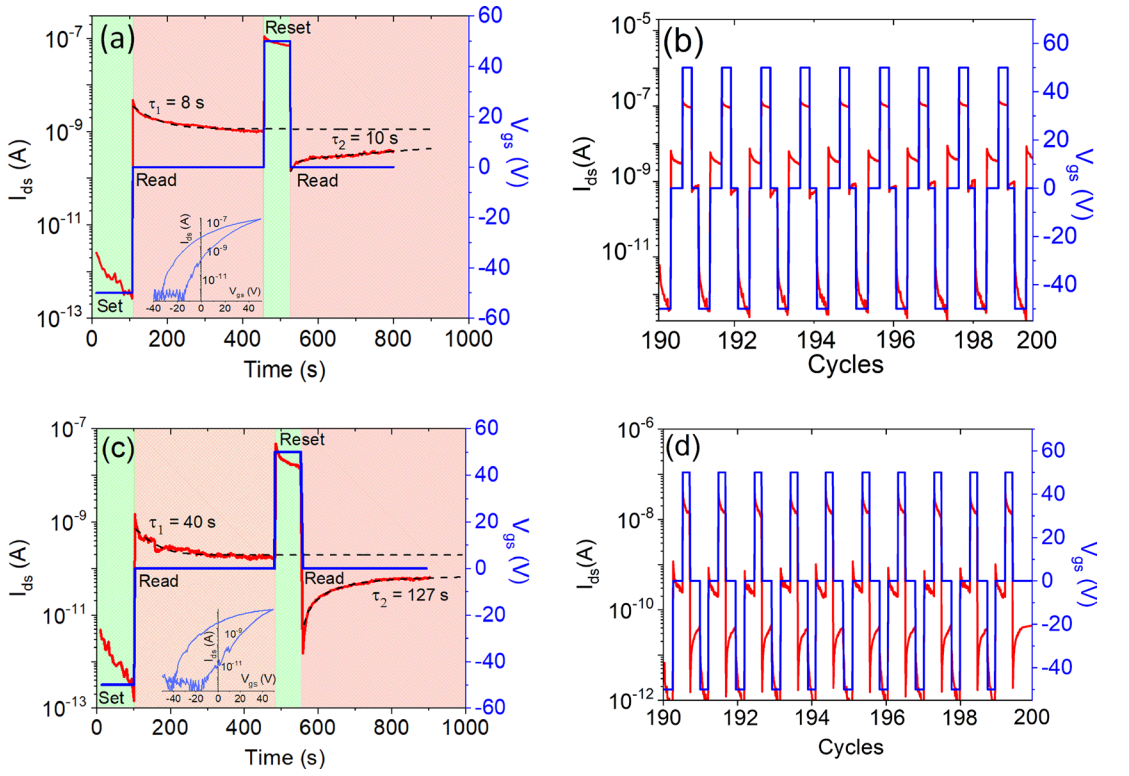

Figure 5. Single and multiple set-read-reset-read cycles for measurements performed (a) and (b) in vacuum ($\sim 10^{-6}$ Torr) and under N_2 atmosphere at a pressure of 760 Torr (c) and (d).

between the total energy of the system (E_{MoS_2+gas}) and that of MoS_2 and the gas phase molecules alone (E_{MoS_2} and E_{gas} respectively)

$$E_{ads} = E_{MoS_2+gas} - E_{MoS_2} - E_{gas}.$$

The adsorption energies were calculated through computational methods (DFT and *ab initio* studies), and the more negative is the adsorption energy the stronger is the interaction with MoS_2, that is the stability of the MoS_2 + gas system [31, 42, 43, 52–55].

The hysteresis width, evaluated at 10^{-11} A in figure 4(c), as a function of the adsorption energy is displayed in figure 4(d).

The adsorption of Ar on MoS_2 has not been clearly investigated to date; for display purpose, we assumed $E_{ads} = 1$ meV in figure 4(d). Ar could contribute to hysteresis, the width of which shows an increase of about 15 V with respect to vacuum, either by adsorption or by increasing the adhesion of the MoS_2 flake on the substrate, as pure pressure effect at 760 Torr [52], which increments the role of the interfacial and SiO_2 traps.

The comparison between transfer characteristics in different gas atmospheres (figure 4(c)) reveals that oxygen, nitrogen, hydrogen and methane strongly affect the MoS_2 electrical features, with a monotonic trend of H_W. This feature points to the suitability of MoS_2 FETs for gas sensing. Such an application is also corroborated by the observation that the effect of gases is reversible. Indeed, figures 4(e) and (f) show that the transfer characteristic modified by the injection of a gas (H_2 in the example) returns about to the initial state when vacuum is restored.

The effect of H_2 on MoS_2 nanostructures has been reported in connection with hydrogen storage application [42], while the effect of CH_4 has been anticipated by DFT studies dealing with low-defective few-layer MoS_2 crystals [43, 54]. Indeed, the adsorption of CH_4 on the MoS_2 channel of the device under study confirms the presence of defects, since DTF study indicate positive adsorption energy (i.e. repulsion) of CH_4 on perfect monolayer MoS_2 [43]. Defects play an important role in the $H_W - |E_{ads}|$ relationship, as gas molecules are mainly adsorbed at the lattice defect sites, because of dangling bonds. The higher is the adsorption energy, the stronger is the interaction of the adsorbed molecules with MoS_2 lattice, which favors the charge exchange that is cause of hysteresis. Furthermore, dissociated and non-dissociated molecules act differently on MoS_2 electronic structure. Non-dissociated molecules, like H_2 and N_2, adsorbed on the MoS_2 surface, define additional trap centers without changing the band-structure. Conversely, dissociated molecules like O_2 modify the MoS_2 band structure by adding inter-band states [57]. Moreover, the adsorption of CH_4 on MoS_2 surface generates a d-MoS_2/p-CH_4 orbital coupling, inducing a net transfer of charge [43].

Finally, we show that the hysteresis in transfer characteristic can be exploited to realize a memory device. Figure 5 reports measurements for single and multiple set-read-reset-read cycles, both in vacuum ($\sim 10^{-6}$ Torr) and at atmospheric pres-

sure. Figures 5(a) and (c) demonstrate that there is an order of magnitude current-level separation after ±50 V gate pulses and that the memory window (which is the separation between the two current levels) is kept constant after two hundred cycles (figures 5(b) and (d)).

The device displays better performance under N_2 atmosphere, with more separated current levels. This suggests that annealing in selected gas environments can be a valid pretreatment in the fabrication of MoS_2 encapsulated devices, such as the ones covered by Al_2O_3 [37], which are obviously more suitable for practical memory applications.

Conclusions

We have presented the electrical transport characterization of FET with monolayer MoS_2 channel. The conductance shows an *n*-type behavior, with prevailing on-state over a wide voltage range and an intrinsic hysteretic behavior. Hysteresis has been investigated as a function of the range and the sweeping rate of the gate-voltage and has suggested that faster and slower components are involved, which are attributed to MoS_2 defects and SiO_2 traps, respectively. Most importantly, we have reported the effect of gas pressure and type on the transfer characteristics of the transistor. We have demonstrated that gas molecules can be adsorbed on defective MoS_2 surface, causing an increment of the hysteresis correlated with the adsorption energy of the system. Finally, we have confirmed the suitability of MoS_2 transistors as memory devices, especially when gases are stably adsorbed on the channel.

Acknowledgments

We acknowledge financial support by POR Campania FSE 2014–2020, Asse III Ob. Specifico l4, Avviso pubblico decreto dirigenziale n. 80 del 31/05/2016. We acknowledge support from the DFG by funding SCHL 384/20-1 (project number 406129719) and NU-TEGRAM (SCHL 384/16-1, projectnumber 279028710).

Conflicts of interest

The authors declare no conflict of interest.

ORCID iDs

Francesca Urban https://orcid.org/0000-0003-2109-1370
Filippo Giubileo https://orcid.org/0000-0003-2233-3810
Alessandro Grillo https://orcid.org/0000-0002-8909-9865
Laura Iemmo https://orcid.org/0000-0002-5111-3887
Giuseppe Luongo https://orcid.org/0000-0002-9071-2647
Maurizio Passacantando https://orcid.org/0000-0002-3680-5295
Lukas Madauß https://orcid.org/0000-0003-2556-5967
Erik Pollmann https://orcid.org/0000-0002-3961-0426
Marika Schleberger https://orcid.org/0000-0002-5785-1186
Antonio Di Bartolomeo https://orcid.org/0000-0002-3629-726X

References

[1] Zhou Z and Yap Y K 2017 Two-dimensional electronics and optoelectronics: present and future *Electronics* **6** 53
[2] Lin Z *et al* 2016 2D materials advances: from large scale synthesis and controlled heterostructures to improved characterization techniques, defects and applications *2D Mater.* **3** 042001
[3] Di Bartolomeo A, Genovese L, Giubileo F, Iemmo L, Luongo G, Tobias Foller and Schleberger M 2018 Hysteresis in the transfer characteristics of 2 transistors *2D Mater.* **5** 015014
[4] Yoon Y, Ganapathi K and Salahuddin S 2011 How good can monolayer MoS_2 transistors be? *Nano Lett.* **11** 3768
[5] Late D J, Shaikh P A, Khare R, Kashid R V, Chaudhary M, More M A and Ogale S B 2014 Pulsed laser-deposited MoS_2 thin films on W and Si: field emission and photoresponse studies *ACS Appl. Mater. Interfaces* **6** 15881
[6] Lopez-Sanchez O, Lembke D, Kayci M, Radenovic A and Kis A 2013 Ultrasensitive photodetectors based on monolayer MoS_2 *Nat. Nanotechnol.* **8** 497
[7] Zhou C, Wang X, Raju S, Lin Z, Villaroman D, Huang B, Chan H L-W, Chan M and Chai Y 2015 Low voltage and high ON/OFF ratio field-effect transistors based on CVD MoS_2 and ultra high-k gate dielectric PZT *Nanoscale* **7** 8695
[8] Nourbakhsh A, Zubair A, Joglekar S, Dresselhaus M and Palacios T 2017 Subthreshold swing improvement in MoS_2 transistors by the negative-capacitance effect in a ferroelectric Al-doped-HfO_2/HfO_2 gate dielectric stack *Nanoscale* **9** 6122
[9] Radisavljevic B, Radenovic A, Brivio J, Giacometti V and Kis A 2011 Single-layer MoS_2 transistors *Nat. Nanotechnol.* **6** 147
[10] Radisavljevic B and Kis A 2013 Mobility engineering and a metal–insulator transition in monolayer MoS_2 *Nat. Mater.* **12** 815
[11] Yin Z, Li H, Li H, Jiang L, Shi Y, Sun Y, Lu G, Zhang Q, Chen X and Zhang H 2012 Single-layer MoS_2 phototransistors *ACS Nano* **6** 74
[12] Huo N, Yang Y, Wu Y-N, Zhang X-G, Pantelides S T and Konstantatos G 2018 High carrier mobility in monolayer CVD-grown MoS_2 through phonon suppression *Nanoscale* **10** 15071–7
[13] Tong X, Ashalley E, Lin F, Li H and Wang Z M 2015 Advances in MoS_2-based field effect transistors (FETs) *Nano-Micro Lett.* **7** 203
[14] Wu W, De D, Chang S-C, Wang Y, Peng H, Bao J and Pei S-S 2013 High mobility and high on/off ratio field-effect transistors based on chemical vapor deposited single-crystal MoS_2 grains *Appl. Phys. Lett.* **102** 142106
[15] Liu H, Neal A T and Ye P D 2012 Channel length scaling of MoS_2 MOSFETs *ACS Nano* **6** 8563
[16] Illarionov Y Y, Knobloch T, Waltl M, Rzepa G, Pospischil A, Polyushkin D K, Furchi M M, Mueller T and Grasser T 2017 Energetic mapping of oxide traps in MoS_2 field-effect transistors *2D Mater.* **4** 025108
[17] Martinez L M, Pinto N J, Naylor C H and Johnson A T C 2016 MoS_2 based dual input logic AND gate *AIP Adv.* **6** 125041

[18] Wachter S, Polyushkin D K, Bethge O and Mueller T 2017 A microprocessor based on a two-dimensional semiconductor *Nat. Commun.* **8** 14948
[19] Di Bartolomeo A, Genovese L, Foller T, Giubileo F, Luongo G, Luca Croin, Liang S-J, Ang L K and Schleberger M 2017 Electrical transport and persistent photoconductivity in monolayer MoS_2 phototransistors *Nanotechnology* **28** 214002
[20] Zibouche N, Kuc A, Musfeldt J and Heine T 2014 Transition-metal dichalcogenides for spintronic applications *Ann. Phys., Lpz.* **526** 395
[21] Han W 2016 Perspectives for spintronics in 2D materials *APL Mater.* **4** 032401
[22] Di Bartolomeo A, Urban F, Passacantando M, McEvoy N, Peters L, Iemmo L, Luongo G, Romeo F and Giubileo F 2019 A WSe_2 vertical field emission transistor *Nanoscale* **11** 1538
[23] Suryawanshi S R, More M A and Late D J 2016 Exfoliated 2D black phosphorus nanosheets: field emission studies *J. Vac. Sci. Technol.* B **34** 041803
[24] Giubileo F, Di Bartolomeo A, Iemmo L, Luongo G, Passacantando M, Koivusalo E, Hakkarainen T V and Guina M 2017 Field emission from self-catalyzed GaAs nanowires *Nanomaterials* **7** 275
[25] Urban F, Passacantando M, Giubileo F, Iemmo L and Di Bartolomeo A 2018 Transport and field emission properties of MoS_2 bilayers *Nanomaterials* **8** 151
[26] Di Bartolomeo A, Giubileo F, Iemmo L, Romeo F, Russo S, Unal S, Passacantando M, Grossi V and Cucolo A M 2016 Leakage and field emission in side-gate graphene field effect transistors *Appl. Phys. Lett.* **109** 023510
[27] Giubileo F, Grillo A, Passacantando M, Urban F, Iemmo L, Luongo G, Pelella A, Loveridge M, Lozzi L and Di Bartolomeo A 2019 Field emission characterization of MoS_2 nanoflowers *Nanomaterials* **9** 717
[28] Grillo A, Barrat J, Galazka Z, Passacantando M, Giubileo F, Iemmo L, Luongo G, Urban F, Dubourdieu C and Di Bartolomeo A 2019 High field-emission current density from β-Ga_2O_3 nanopillars *Appl. Phys. Lett.* **114** 193101
[29] Giubileo F, Iemmo L, Passacantando M, Urban F, Luongo G, Sun L, Amato G, Enrico E and Di Bartolomeo A 2019 Effect of electron irradiation on the transport and field emission properties of few-layer MoS_2 field-effect transistors *J. Phys. Chem.* C **123** 1454
[30] Li H, Yin Z, He Q, Li H, Huang X, Lu G, Fam D W H, Tok A I Y, Zhang Q and Zhang H 2012 Fabrication of single- and multilayer MoS_2 film-based field-effect transistors for sensing NO at room temperature *Small* **8** 63
[31] Yue Q, Shao Z, Chang S and Li J 2013 Adsorption of gas molecules on monolayer MoS_2 and effect of applied electric field *Nanoscale Res. Lett.* **8** 425
[32] Ferreira F, Carvalho A, Moura Í J M, Coutinho J and Ribeiro R M 2017 Adsorption of H_2, O_2, H_2O, OH and H on monolayer MoS_2 *J. Phys.: Condens. Matter* **30** 035003
[33] Urban F, Martucciello N, Peters L, McEvoy N and Di Bartolomeo A 2018 Environmental effects on the electrical characteristics of back-gated WSe_2 field-effect transistors *Nanomaterials* **8** 901
[34] Di Bartolomeo A, Pelella A, Liu X, Miao F, Passacantando M, Giubileo F, Grillo A, Iemmo L, Urban F and Liang S-J 2019 Pressure-tunable ambipolar conduction and hysteresis in thin palladium diselenide field effect transistors *Adv. Funct. Mater.* **29** 1902483
[35] Xu Q, Sun Y, Yang P and Dan Y 2019 Density of defect states retrieved from the hysteretic gate transfer characteristics of monolayer MoS_2 field effect transistors *AIP Adv.* **9** 015230
[36] Shimazu Y, Tashiro M, Sonobe S and Takahashi M 2016 Environmental effects on hysteresis of transfer characteristics in molybdenum disulfide field-effect transistors *Sci. Rep.* **6** 30084
[37] Zhang E, Wang W, Zhang C, Jin Y, Zhu G, Sun Q, Zhang D W, Zhou P and Xiu F 2015 Tunable charge-trap memory based on few-layer MoS_2 *ACS Nano* **9** 612
[38] Di Bartolomeo A, Rücker H, Schley P, Fox A, Lischke S and Na K-Y 2009 A single-poly EEPROM cell for embedded memory applications *Solid-State Electron.* **53** 644
[39] Di Bartolomeo A, Yang Y, Rinzan M B M, Boyd A K and Barbara P 2010 Record endurance for single-walled carbon nanotube-based memory cell *Nanoscale Res. Lett.* **5** 1852
[40] Mak K F, Lee C, Hone J, Shan J and Heinz T F 2010 Atomically thin MoS_2: a new direct-gap semiconductor *Phys. Rev. Lett.* **105** 136805
[41] Tsai M-L, Su S-H, Chang J-K, Tsai D-S, Chen C-H, Wu C-I, Li L-J, Chen L-J and He J-H 2014 Monolayer MoS_2 heterojunction solar cells *ACS Nano* **8** 8317
[42] Wang X, Li B, Bell D R, Li W and Zhou R 2017 Hydrogen and methane storage and release by MoS_2 nanotubes for energy storage *J. Mater. Chem.* A **5** 23020
[43] Yu N, Wang L, Li M, Sun X, Hou T and Li Y 2015 Molybdenum disulfide as a highly efficient adsorbent for non-polar gases *Phys. Chem. Chem. Phys.* **17** 11700
[44] Di Bartolomeo A *et al* 2018 Asymmetric Schottky contacts in bilayer MoS_2 field effect transistors *Adv. Funct. Mater.* **28** 1800657
[45] Kim C, Moon I, Lee D, Choi M S, Ahmed F, Nam S, Cho Y, Shin H-J, Park S and Yoo W J 2017 Fermi level pinning at electrical metal contacts of monolayer molybdenum dichalcogenides *ACS Nano* **11** 1588–96
[46] Giubileo F and Di Bartolomeo A 2017 The role of contact resistance in graphene field-effect devices *Prog. Surf. Sci.* **92** 143
[47] Cho K, Park W, Park J, Jeong H, Jang J, Kim T-Y, Hong W-K, Hong S and Lee T 2013 Electric stress-induced threshold voltage instability of multilayer MoS_2 field effect transistors *ACS Nano* **7** 7751–8
[48] Late D J, Liu B, Matte H S S R, Dravid V P and Rao C N R 2012 Hysteresis in single-layer MoS_2 field effect transistors *ACS Nano* **6** 5635
[49] Maeng J, Park W, Choe M, Jo G, Kahng Y H and Lee T 2009 Transient drain current characteristics of ZnO nanowire field effect transistors *Appl. Phys. Lett.* **95** 123101
[50] Lee Y G, Kang C G, Jung U J, Kim J J, Hwang H J, Chung H-J, Seo S, Choi R and Lee B H 2011 Fast transient charging at the graphene/SiO_2 interface causing hysteretic device characteristics *Appl. Phys. Lett.* **98** 183508
[51] Ahn J-H, Parkin W M, Naylor C H, Johnson A T C and Drndić M 2017 Ambient effects on electrical characteristics of CVD-grown monolayer MoS_2 field-effect transistors *Sci. Rep.* **7** 4075
[52] Lloyd D, Liu X, Boddeti N, Cantley L, Long R, Dunn M L and Bunch J S 2017 Adhesion, stiffness, and instability in atomically thin MoS_2 bubbles *Nano Lett.* **17** 5329
[53] Kronberg R, Hakala M, Holmberg N and Laasonen K 2017 Hydrogen adsorption on MoS_2-surfaces: a DFT study on preferential sites and the effect of sulfur and hydrogen coverage *Phys. Chem. Chem. Phys.* **19** 16231
[54] Li H, Huang M and Cao G 2016 Markedly different adsorption behaviors of gas molecules on defective monolayer MoS_2: a first-principles study *Phys. Chem. Chem. Phys.* **18** 15110
[55] Cho B *et al* 2015 Charge-transfer-based gas sensing using atomic-layer MoS_2 *Sci. Rep.* **5** 8052
[56] Kysilka J, Rubeš M, Grajciar L, Nachtigall P and Bludský O 2011 Accurate description of argon and water adsorption on surfaces of graphene-based carbon allotropes *J. Phys. Chem.* A **115** 11387–93
[57] Cha J, Min K-A, Sung D and Hong S 2018 *Ab initio* study of adsorption behaviors of molecular adsorbates on the surface and at the edge of MoS_2 *Curr. Appl. Phys.* **18** 1013–9